J Mater Sci (2009) 44:1082–1093
DOI 10.1007/s10853-008-3195-8

Study of wear behaviour of austempered ductile iron

U. Ritha Kumari · P. Prasad Rao

Received: 16 February 2008 / Accepted: 15 December 2008 / Published online: 14 January 2009

Abstract An investigation was carried out to examine the influence of austempering temperature on microstructural parameters and the wear behaviour of austempered ductile iron. Ductile iron was austenitised at 900 °C for 30 min and austempered for 2 h at 260, 280, 300, 320, 350, 380 and 400 °C. Resulting microstructures were characterised through optical microscopy and X-ray diffraction. Wear test was carried out using a pin-on-disc machine with sliding speed of 289 m min^{-1}. Coarse ausferrite microstructure exhibited higher wear rate than fine ausferrite microstructure. At high austempering temperature large amounts of austenite was instrumental in improving the wear resistance through formation of deformation induced martensite. Study of the wear surface under scanning electron microscope showed that, under dry sliding condition, wear occurred mainly due to adhesion and delamination. Wear rate was found to be dependent on the yield strength, austenite content and its carbon content.

Introduction

When a ductile cast iron is subjected to austempering heat treatment an interesting microstructure is obtained which consists of ferrite and high carbon austenite. This is unlike the microstructure of austempered steel which consists of ferrite and carbide. The microstructure consisting of ferrite and austenite in austempered ductile iron (ADI) is called as ausferrite. During the austempering of ductile cast iron, a variety of microstructures are obtained depending on the heat treatment parameters such as austenitising time and temperature and the austempering time and temperature. When austempered at low temperatures of less than 300 °C, the microstructure consists of very fine ferrite platelets, separated by thin slivers of stabilized austenite. Such a microstructure results in high strength and low ductility. However, when austempered at temperatures greater than 350 °C, coarse ferrite is observed separated from each other by blocky austenite. ADIs with such microstuctures normally exhibit low strength and high ductility. The influence of the heat treatment parameters on the microstructure and the influence of the microstructure on the mechanical properties have been reported by several investigators [1–12]. Interesting microstructural studies have also been carried out on embrittling of ADI when in contact with moisture [13], its stress corrosion cracking behaviour [14] and the influence of welding [15].

Austempered ductile iron has been recognised as an important engineering material because of its excellent properties. These include high strength with good ductility [16–18], good wear resistance [19–21] and good fatigue strength [22–25]. Some examples of its successful application are gears, agricultural implements and automobile and engine parts. Many of these are subjected to sliding and rolling wear [26–29]. However, the research work on the wear of ADI is lagging behind its application. The effect of its microstructure on wear under various working conditions and the wear mechanisms has still not been fully understood.

U. R. Kumari
A.B. Shetty Memorial Institute of Dental Science, Deralakatte, Mangalore, Karnataka, India

P. P. Rao (✉)
Department of Metallurgical and Materials Engineering, National Institute of Technology Karnataka, Surathkal, Mangalore 575025, Karnataka, India
e-mail: ppr@nitk.ac.in

Wear resistance is an important mechanical property. Investigations [30, 31] have shown that ADI possesses better wear resistance than cast iron. Ahmadabadi et al. [32] also observed that wear resistance of ADI was higher than that of the grey cast iron. They concluded that higher wear resistance of ADI was due to the presence of ferrite and high carbon austenite. It has been reported [33–35] that enhanced wear resistance in ADI is due to the ability of the austenite to strain harden and also due to the formation of strain induced martensite. Austempered ductile cast iron exhibits better wear resistance as compared to the martensitic steels with similar hardness, depending on the tribosystem [36]. Even the low hardness ADI presents good abrasion resistance if strain induced martensite or strain hardening occur [37]. Velez [38] showed that ADIs with fine ausferrite show greater wear resistance than quenched and tempered irons of the same hardness. He related this to a significant strain hardening of austenite or to strain induced martensitic transformation.

Mohan et al. [39] too reported greater abrasive wear resistance for fine ausferrite matrix, as compared to tempered martensite matrix with same hardness. The high volume fraction of high carbon austenite characteristic of the ausferrite structure of these materials can explain this behaviour. The ductility and strain hardening capability of this austenite or its strain induced martensite transformation produces a considerable increase in the hardness. Zhou et al. [40] found that abrasive wear resistance of the ductile cast iron with martensite matrix also depends on the austenite volume fraction. It is pertinent to point out here that the influence of the morphology of the microstructure on the formation of strain induced martensite has been investigated by Daber and Rao [41] and also by Daber et al. [42]. They reported that blocky martensite produced at higher austempering temperatures is prone to undergo strain induced transformation to martensite. They also exhibited this through a two step austempering where the ADI had a mixed microstructure consisting of fine ausferrite produced at low austempering temperatures and coarse ausferrite produced at high austempering temperatures. The wear behaviour of austempered ductile cast iron containing aluminium was studied by Boutorabi et al. [43]. They showed that it is a complex function of austempering temperature and time. Ahmadabadi [44] has reported that ADI with 0.75 wt% Mn austempered at 315 °C has the higher wear resistance than that austempered at 375 °C. He also showed that specimen with lower nodule count have lower wear rate than specimen with higher nodule count. The present investigation has been undertaken to study the wear rate of ADI under different austempering temperatures and to study the influence of microstructure on wear rate.

Experimental work

Material

The ductile cast iron used in the present investigation was cast in the form of slabs of dimension 200 mm × 150 mm × 30 mm. The chemical composition of the ductile iron is shown in Table 1. The present composition was chosen because iron with similar chemistry had been used in our laboratories in previous studies, and hence considerable data on microstructure, mechanical properties and fracture toughness are available on it. It was therefore decided to carry out the wear study also on ductile cast iron of the same composition. It should be noted that such a heavily alloyed ductile iron is not generally needed for ADI in commercial applications to get through hardening. Nodularity and nodule count were carried out through image analysis software. The average nodularity was 95% and the average nodule count was 103 mm^{-2}.

Samples of 6 mm diameter and 25 mm length for wear studies and round cylindrical samples with gauge length of 42 mm and diameter of 6 mm for tensile studies were machined from the cast slabs.

All the samples were austenitised at 900 °C for 30 min and then austempered at a selected temperature for 2 h. Seven different temperatures were selected for austempering. These were 260, 280, 300, 320, 350, 380 and 400 °C. These temperatures were selected to cover the complete range of microstructures from fine ausferrite to coarse ausferrite.

Microstructures of the heat-treated samples were studied qualitatively by optical microscopy after etching with 5% nital. Quantitative information on the microstructure was obtained through X-ray diffraction. XRD studies were carried out on a JEOL-JDX-8P diffractometer using copper K_α radiation with nickel filter. The tube voltage was 30 kV and tube current was 20 mA. A scan speed of 0.25 degree per minute was employed over an angular 2θ range of 42–46°. Two peaks were obtained within this angular range: the (111) peak of the austenite and the (110) peak of the

Table 1 Chemical composition of the ductile iron

Element	Weight percent
Carbon	3.5
Silicon	2.5
Manganese	0.3
Sulphur	0.1
Phosphorous	0.02
Nickel	1.5
Molybdenum	0.3
Copper	0.5

ferrite. The profiles were analysed with a computer to obtain the peak position as well as the integrated intensity of austenite and ferrite peaks.

The volume fraction of austenite was determined by Cullity's direct comparison method [45, 46]. From diffraction profiles, peak positions, as well as the integrated intensities of austenite and ferrite peaks were measured. Assuming that ferrite and austenite were the only matrix phases present, the ratio of the integrated intensities of the diffraction peaks from these phases can be written as

$$\frac{I_\gamma}{I_\alpha} = \frac{R_\gamma}{R_\alpha} \cdot \frac{X_\gamma}{X_\alpha} \tag{1}$$

where, I_γ is the integrated intensity from a given (hkl) plane of the γ phase; I_α is the integrated intensity from a given (hkl) plane of the α phase; X_γ is the volume fraction of austenite; X_α is the volume fraction of ferrite; and the constants R_γ and R_α are given by the following expression for each peak:

$$R = [1/V^2][F \cdot p \cdot (LP)]e^{-2m} \tag{2}$$

where, V is the atomic volume of unit cell; F is the structure factor; p is the multiplicity factor; LP is the Lorentz Polarisation factor; and e^{-2m} is the temperature factor.

The carbon content of the austenite was estimated quantitatively by X-ray diffraction technique using the following relationship [47] between its lattice parameter and the carbon content:

$$a_\gamma = 0.3548 + 0.0044C_\gamma \tag{3}$$

where, a_γ is the lattice parameter of austenite in nanometer and C_γ is its carbon content in weight percent. The Bragg angle obtained from the (111) peak of austenite was used in estimating the lattice parameter.

Hardness of all the heat treated samples was determined on a Zwick Vickers hardness tester using a load of 5 kg. Ten readings were taken on each sample and the results reported are an average of these 10 readings. Tensile testing was conducted on an Instron machine (model 4206) at a constant crosshead speed of 1 mm/min. Ultimate tensile strength, 0.2% offset yield strength and percentage elongation were estimated. Five samples were tested for each heat treatment condition and the values reported are the average of these five tests.

Wear tests were carried out on a Ducon make pin-on-disc type of machine, which works on the principle of sliding cantilever. This machine is designed to study the unlubricated sliding wear as a function of load and speed. A variable speed motor rotates the wear disc that is connected to the vertical shaft of the motor. The wear disc was made of En31 steel, heat-treated to a hardness of 65 HRC. The disc was rotated at a constant speed of 920 rpm. The speed of the disc at the point of contact with the pin was 289 m min^{-1}. The circular surface of the pin was pressed on the horizontal rotating disc with a normal stress of 23 MPa. Test durations were 120 min. The difference in weight before and after the wear test was used to determine the weight loss. The weight loss per unit area per unit time under different austempering conditions was measured. Six samples were tested for each heat treatment condition and the wear rate reported is an average of these six readings. The worn surfaces were studied under LEO 440i SEM with oxford EDAX facility, for identifying the nature of distortion at the surface.

Results and discussion

Microstructure

Ductile iron on quenching from the austempering temperature exhibits a microstructure consisting of bainitic ferrite in a matrix of high carbon austenite. Such a microstructure is called as ausferrite. This is the desired microstructure of ADI. The morphology of the bainitic ferrite, the austenite content and the carbon content of the austenite varies with austempering temperature. The austempered specimens in the present work were studied by optical microscopy to establish the morphology of the bainitic ferrite. X-ray diffraction analysis was carried out to ascertain the amount of austenite and its carbon content.

Optical microscopy

The microstructures of the samples obtained at different austempering temperatures, in the present investigation, was found to compare well with those reported by earlier investigators [48]. A systematic variation in the microstructure was seen from very fine ferrite with little austenite (at 260 °C) to coarse ferrite with a large amount of austenite (at 400 °C). At lower temperatures of 260–320 °C, the microstructure consisted of very fine ferrite needles with thin layers of austenite between them. These microstructures are presented in Fig. 1. At higher austempering temperatures of 350–400 °C, the microstructure consisted of very coarse and feathery ferrite with relatively large amount of bulky austenite. At the highest temperature of 400 °C, coarse ferrite well separated from each other by wide areas of austenite was observed. Thus, increasing the austempering temperature resulted in coarsening of the ferrite, as well as, an increase in the austenite content. These microstructures are presented in Fig. 2.

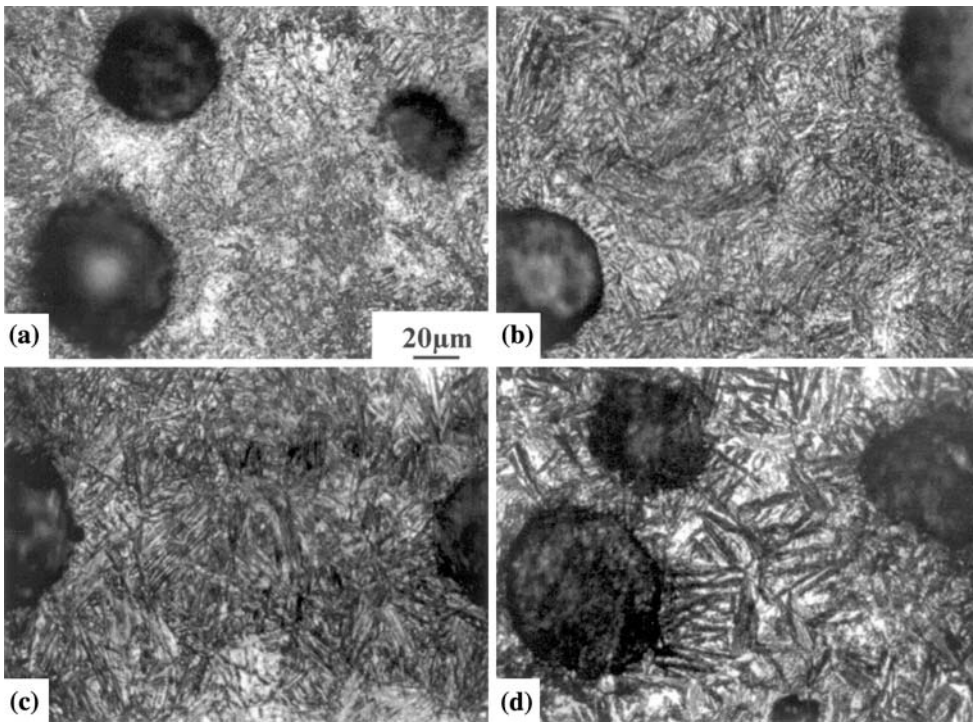

Fig. 1 Microstructures of ADI austempered for 2 h at **a** 260 °C, **b** 280 °C, **c** 300 °C and **d** 320 °C

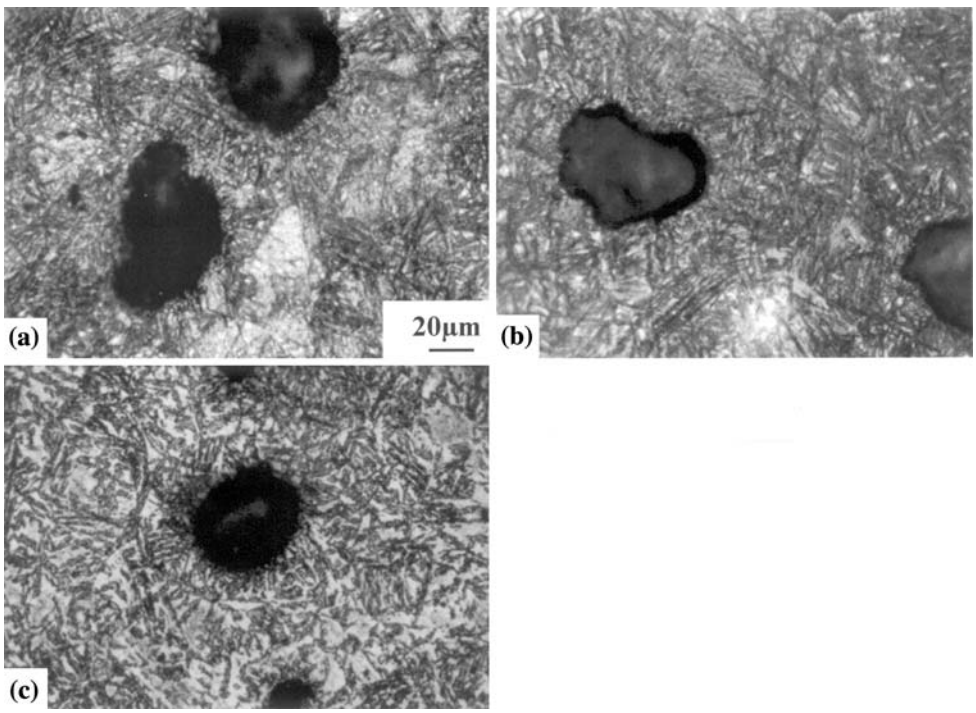

Fig. 2 Microstructures of ADI austempered for 2 h at **a** 350 °C, **b** 380 °C, and **c** 400 °C

X-ray diffraction studies

While the optical microscopy gave a qualitative picture of the microstructural evolution, quantitative information was obtained through the X-ray diffraction technique. Using the XRD profiles, volume fraction of austenite at different austempering temperatures and times was estimated. Figure 3 shows the variation of the volume fraction of austenite, X_γ, with austempering temperature. These samples were austempered for 2 h at the respective temperature. It was observed that the volume fraction of the austenite increased steadily from 15 to 41% as the austempering temperature was increased from 260 °C to 400 °C. The diffusion of carbon from the regions

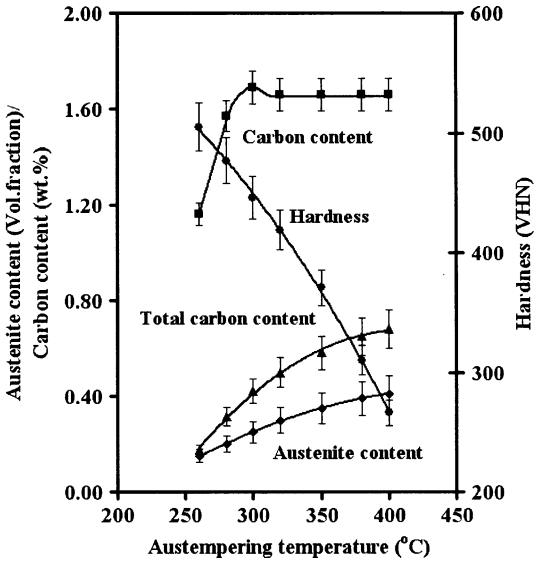

Fig. 3 Variation of volume fraction of austenite, carbon content, total carbon content and hardness with austempering temperature

transforming into ferrite to the surrounding austenite increases as the austempering temperature is increased. Thus at a given austempering time, there is more austenite at the higher temperature. The variation in the austenite content observed in the present investigation is similar to that observed by Rundman and Klug [45]. They observed larger amount of austenite because of higher austenitising temperatures employed by them. Their results at the lowest austenitising temperature of 900 °C are comparable with those of the present work.

Another important microstructural feature is the carbon content of the austenite. This was estimated by using Eq. 3. The influence of the austempering temperature on the carbon content of the austenite is presented in Fig. 3. The carbon content was very low, about 1.16 wt%, when the sample was austempered at a low temperature of 260 °C. This rapidly rose to nearly 1.7 wt% when austempered at 300 °C. Beyond this temperature, the carbon content decreased slightly and reached a constant value with increasing temperature. At the low temperatures, because of the low diffusion rate and the fast kinetics of the ferrite formation, little carbon diffuses into the austenite. Hence the carbon content will be low. As the temperature is raised, more carbon finds its way into the surrounding austenite from the regions transforming to ferrite due to the higher diffusion rates as well as the slower kinetics of ferrite formation at decreasing supercooling. The influence of the austempering temperature on the total carbon content of the austenite is presented in Fig. 3. It was found that total carbon content was only 0.17 wt% at 260 °C. It rose continuously with increasing austempering temperature to 0.71 wt% at 400 °C. The initial carbon content of the austenite is given by the following relationship due to Voigt and Loper [49]:

$$C_o = \left(\frac{T_\gamma}{420}\right) - 0.17(\mathrm{Si}) - 0.95 \quad (4)$$

where, C_o is the carbon content in wt%, T_γ is the austenitising temperature in °C and Si is the weight percent silicon in the iron. Under the present conditions this works out to 0.77 wt%. Thus it can be seen that, on austempering at 400 °C, most of this finds its way into the austenite, while at 260 °C very little of it enters the austenite.

Mechanical properties

The variation of hardness with austempering temperature is shown in Fig. 3. Maximum hardness was noticed at lower austempering temperature. Fine ausferrite microstructure that forms at lower temperatures has higher hardness than the coarse ausferrite microstructure that forms at higher temperatures. The variation of hardness with austempering temperature observed in the present investigation compared well with those reported by previous investigators [5, 6, 50, 51].

The tensile strength and yield strength were found to decrease monotonically as austempering temperature was increased as shown in Fig. 4. On the other hand, ductility as measured by percent elongation was found to increase. It was observed that the low austempering temperatures resulted in ADI of high strength and low ductility, while the high austempering temperatures resulted in ADI of low strength and high ductility. The sample austempered at 260 °C exhibited a tensile strength of 1,613 MPa and a yield strength of 1,315 MPa. These decreased to 800 MPa and 601 MPa, respectively, on austempering at 400 °C.

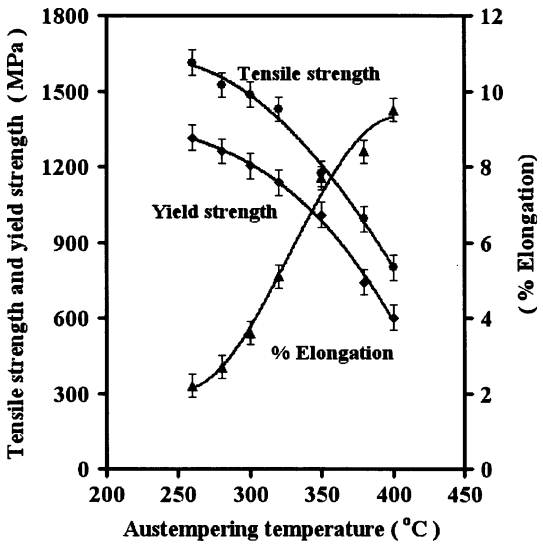

Fig. 4 Variation of tensile properties with austempering temperature

However, ductility rose from 2.2% at 260 °C to 9.5% at 400 °C. The results of the present investigation compare very favourably with those of the previous investigators [5, 6, 50, 51]. It has been generally concluded that increase in strength with decreasing austempering temperature is due to the refinement of the microstructure. Hayrynen et al. [52] have shown that the yield strength of ADI can be expressed in terms of the ferrite particle size and the austenite content by the following equation:

$$\sigma_y = AL^{-1/2} + BX_\gamma + C \quad (5)$$

where, L is the ferrite particle size, X_γ is the volume fraction of austenite, and A, B and C are constants. The above equation has been shown to be valid by Ali et al. [53] also. Both investigators have shown that ferrite particle size is the dominant factor, and therefore, the yield strength is essentially proportional to $L^{-1/2}$. As shown earlier while discussing the microstructure, the ferrite particle size decreased with decreasing austempering temperature, accounting for the observed dependence of strength on austempering temperature.

The mechanical behaviour of ADIs austempered at different temperatures is controlled by different mechanism. At low temperatures, the fine laths of the ferrite are the determining factor, while at higher temperatures the strain hardening capacity of the austenite that is present in large quantity, is the controlling factor. In order to examine this aspect the strain hardening behaviour of the samples austempered at different temperatures was studied. For this purpose, it was assumed that the flow curves could be expressed by the Hollomon relationship [54].

$$\sigma = K\varepsilon^n \quad (6)$$

where, σ is the stress, ε is the strain, K is the strength coefficient and n is the strain hardening exponent. According to this, a plot of true stress against true strain on a log–log scale should result in a straight line with a slope of n. The stress–strain diagrams obtained during tensile testing were used to plot the true stress–true strain diagrams on a logarithmic scale. These resulted in straight lines confirming validity of Hollomon relationship, as shown in Fig. 5.

Strain hardening exponent was calculated for all samples by measuring slope of the double log plot of true stress against true strain which is shown in Fig. 5. The variation of the strain hardening exponent with austempering temperature is shown in Fig. 6. The strain hardening exponent was found to rise steadily as the austempering temperature was increased. The strain hardening exponent was the maximum when the microstructure consisted of coarse ferrite (austempered at 400 °C) with high austenite content, and minimum when the microstructure had fine ferrite (austempered at 260 °C) with low austenite content.

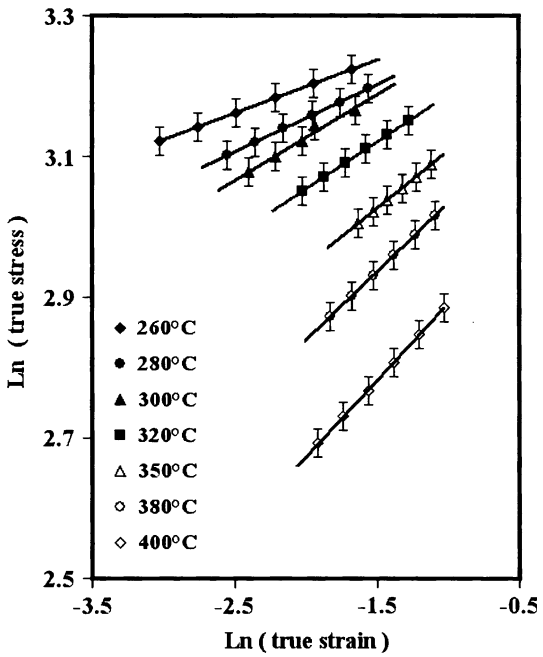

Fig. 5 Log–log plot of true stress against true strain of samples subjected to conventional austempering

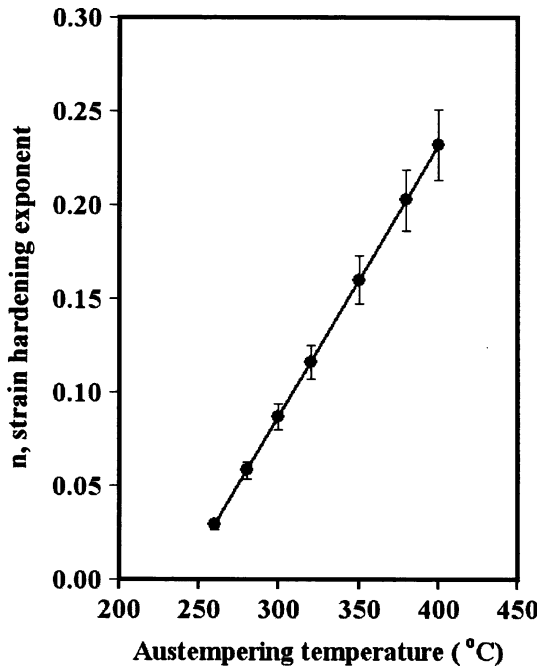

Fig. 6 Variation of strain hardening exponent with austempering temperature

Microstructural studies of the deformed samples were carried out to see if any significant changes occurred. Specimens were cut from tensile samples very close to the fracture surface under all heat treatment conditions, and the microstructures were studied under optical microscope. No significant changes were observed when austempering

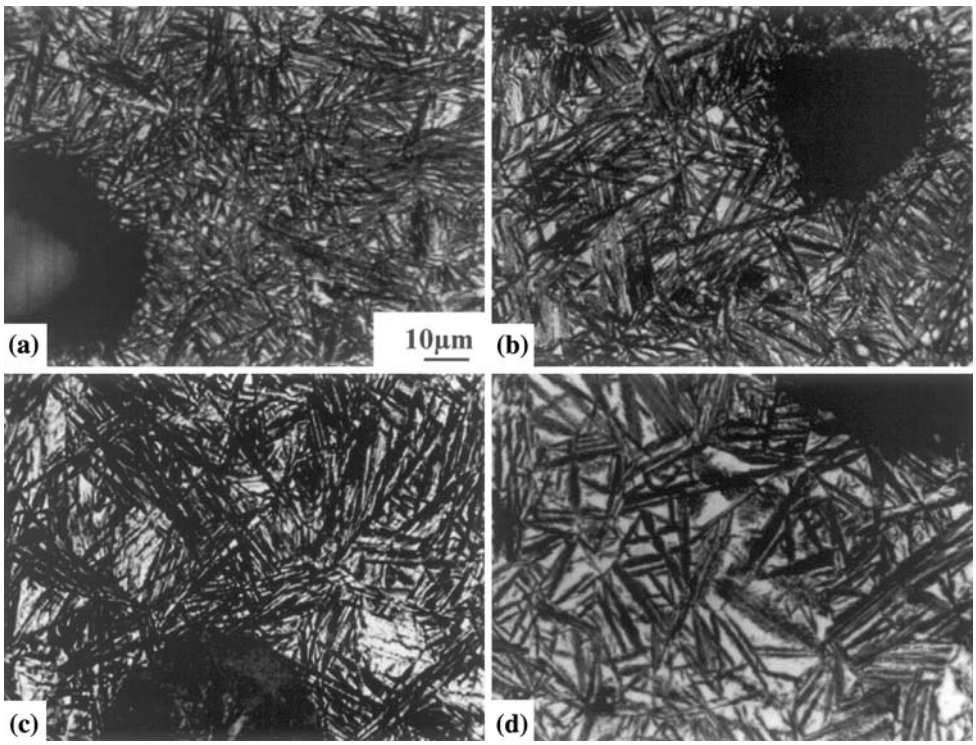

Fig. 7 Microstructures of deformed ADI austempered for 2 h at **a** 260 °C, **b** 280 °C, **c** 300 °C, and **d** 320 °C

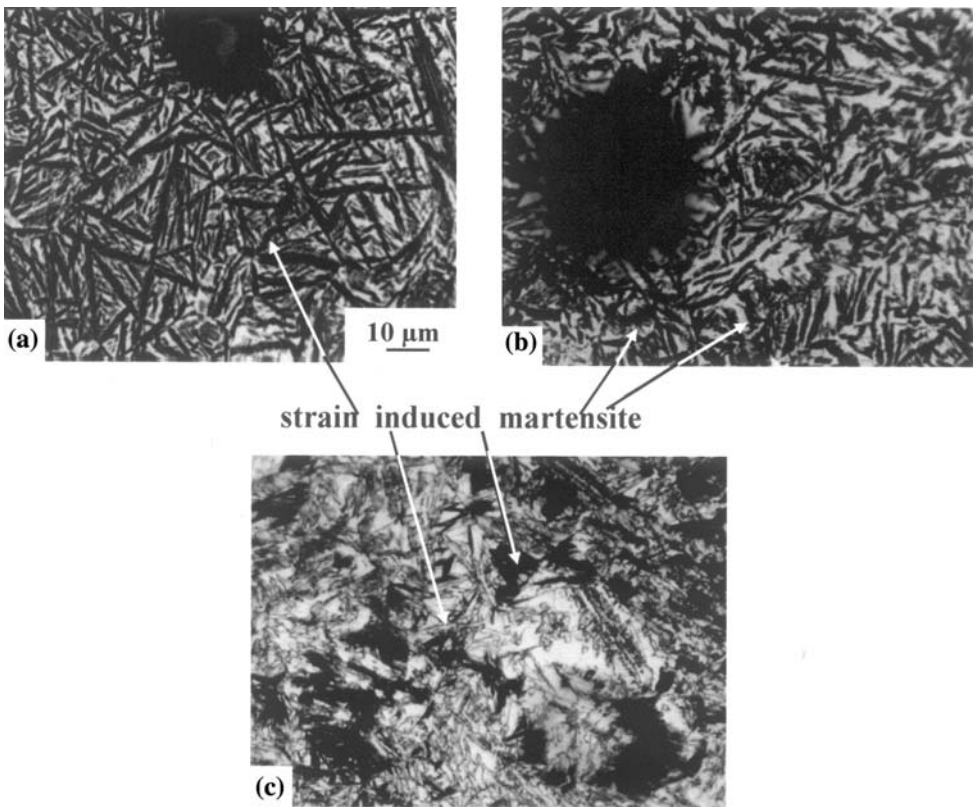

Fig. 8 Microstructures of deformed ADI austempered for 2 h at **a** 350 °C, **b** 380 °C, and **c** 400 °C

temperatures were in the range of 260–320 °C. The microstructures are presented in Fig. 7. These microstructures are identical with those of undeformed samples shown in Fig. 1 However, samples austempered at higher temperatures exhibited some interesting features. Significant presence of martensite could be seen in all of them, as shown in Fig. 8. The sample austempered at the highest temperature of 400 °C shows the maximum extent of

martensite. Dark etching lenticular shaped martensite was present in profusion. Because of the large amount of austenite present in this, which is seen as broad white etching areas, the martensite could be clearly seen in it. Martensite was found within the austenite. Lenticular martensite, linked end to end could be seen all over the sample. At austempering temperatures of 380 and 350 °C, the austenite was less and was present in confined regions between the sheaths of ferrite. Here too martensite needles could be seen but fewer in numbers and smaller in size.

The fact that the austenite transformed to martensite during plastic deformation could be confirmed by measuring the austenite content before and after plastic deformation. In order to do this, X-ray diffraction studies were carried out on the fracture surfaces of the tensile samples, and the amount of the austenite so determined is shown in Fig. 9. The results of the undeformed samples at each temperature are also shown for comparison. At the low austempering temperature of 260 and 280 °C, there was hardly any difference in the austenite contents before and after deformation, indicating that no martensite formed during deformation. However, at higher austempering temperatures of 380 and 400 °C, there was a substantial drop in the austenite content on deforming the sample. For example, in the sample austempered at 400 °C, the fracture surface revealed only about 26 vol.% of austenite as compared to about 41 vol.% in the sample immediately after austempering.

Several parameters influence the stability of the austenite during deformation. These are the carbon content of the austenite [55–57], size [58–61] and morphology [62, 63] of the austenite and its distribution [64] within the microstructure. The chemical driving force for the transformation of austenite to martensite is determined by the carbon content. Austenite containing less than 0.6 wt% carbon is known to transform rapidly to martensite during deformation. In the present investigation, the carbon content is in the range of 1.10–1.70 wt%. Hence, it can be ruled out as an important parameter. Small sized austenite grains less than 1 μm are expected to be highly stable as they contain less potential sites for nucleation of martensite. Such austenite regions will need a greater driving force for nucleation of martensite. Therefore, ADIs austempered at lower temperatures such as 260, 280 and 300 °C will be highly stable during deformation. The austenite in these is present as only thin slivers between ferrite sheaths. Besides, thin films of austenite are more stable than blocky austenite. Thus, on account of size as well as morphology, the strain induced transformation of austenite becomes easier as the austempering temperature is increased. Location of the austenite is another important factor. If martensite is present in the vicinity of austenite, the latter can transform to martensite during early stages of straining. Ferrite can act as a barrier to autocatalytic propagation. Thus, size, morphology and distribution of austenite become increasingly favourable for transformation of austenite to martensite during plastic deformation as the austempering temperature is raised. By all these parameters it can be seen that ausferrite formed at higher temperatures has very low stability under stress, while that formed at lower temperatures has very high stability. This accounts for the extensive presence of martensite in the deformed ADI austempered at higher temperatures. These are in conformity with the results of Daber and Rao [41] as well as those of Daber et al. [42].

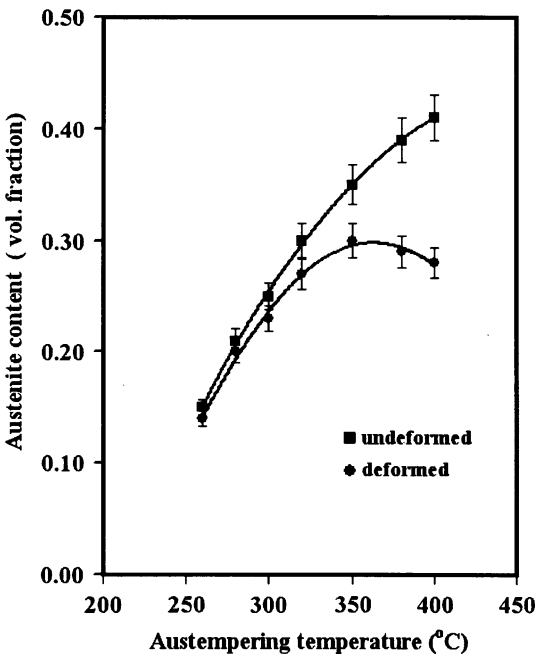

Fig. 9 Variation of volume fraction of austenite with austempering temperature under deformed and undeformed conditions

Wear study

Influence of austempering temperature, hardness and austenite content on the wear rate is presented in Fig. 10. It was found that the samples austempered at 260 °C had the lowest wear rate, and that it increased with increasing austempering temperature. This can be primarily attributed to the decreasing hardness of the ADI due to increasing volume fraction of austenite. It was found that wear rate increased with decreasing hardness and increasing volume fraction of austenite, as shown in Fig. 10.

If hardness is the only parameter controlling the wear rate, the wear rate should have increased by twice going from austempering temperature of 260 to 400 °C, since the hardness halved from about 500 VHN to about 250 VHN. Therefore, there are other factors, which are improving the wear resistance even as hardness is dropping. The

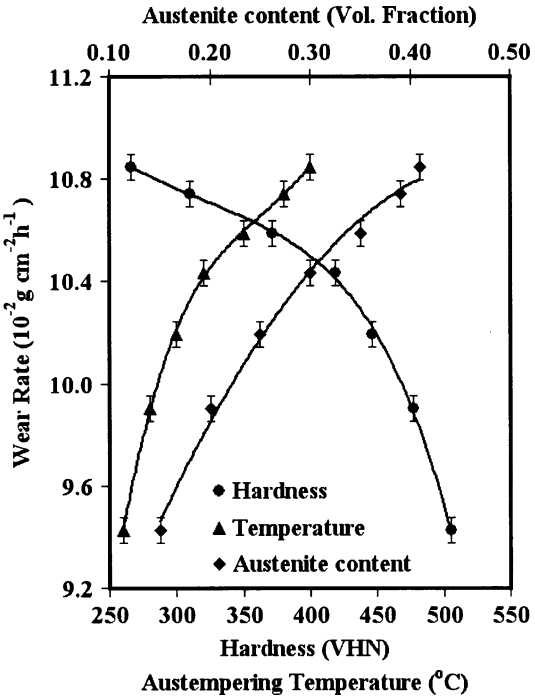

Fig. 10 Influence of austempering temperature, hardness and austenite content on the wear rate

microstructural features such as the morphology, austenite content and its carbon content apparently are playing a crucial role in pulling down the wear rate even as the austempering temperature is increased, and the hardness is dropped.

SEM studies of the worn surfaces were carried out to understand the nature of the wear process. The results of the SEM study also showed that at lower austempering temperatures like 260 and 280 °C, the wear surface primarily consisted of shallow wear scars with small pits as shown in Fig. 11. As the austempering temperature was increased the surface appearance changed markedly to show signs of scuffing and microcracks. With further rise in temperature, there was evidence of extensive plastic flow and tongue formation. These are shown in Fig. 12. All these are tell tale signs of wear by adhesion and delamination.

In the present investigation, the wear occurred due to the contact between the two moving surfaces. One was a hardened steel disc and the other was a small pin pressed against the disc with a constant load. Main component of the wear process would be plastic flow of the material on the pin surface in the direction of rotation, and its eventual tearing from the surface. Because of the high temperature that is generated, and large plastic deformation, adhesion may occur between the two components, followed by tear.

At high temperatures, there may be considerable oxidation of the iron. The iron oxides being brittle, may easily break away from the sample surface. The load is essentially compressive in nature with some shear

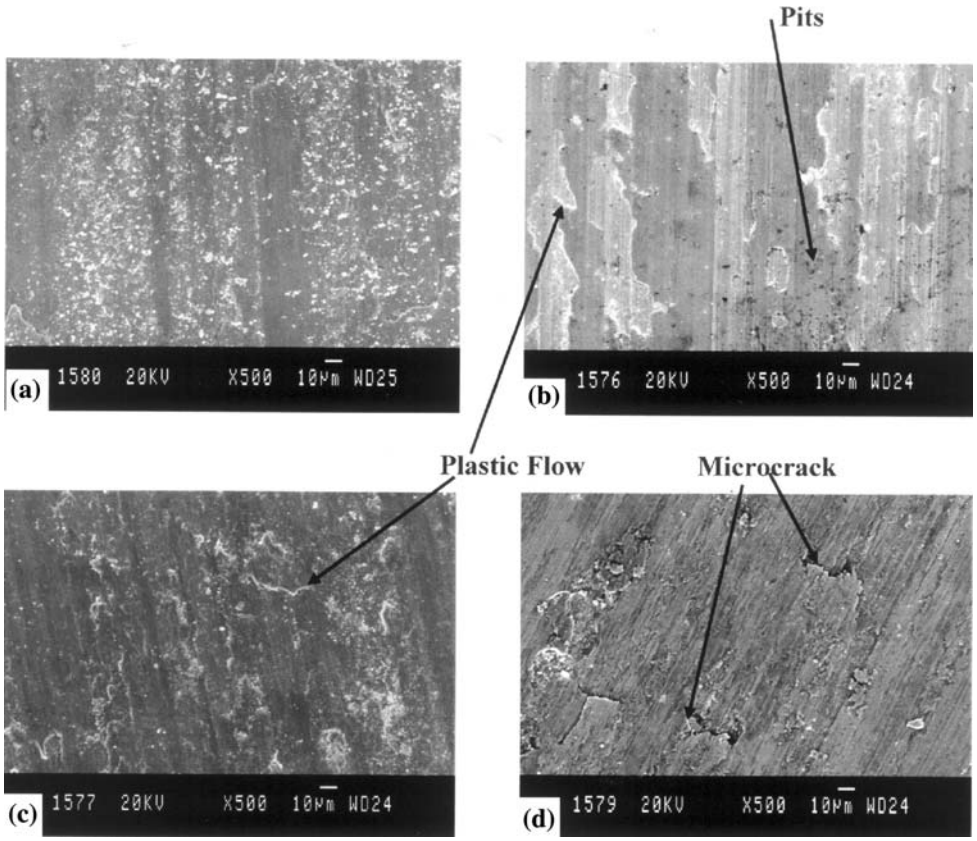

Fig. 11 SEM micrographs of samples subjected to austempering for 2 h at **a** 260 °C, **b** 280 °C, **c** 300 °C and **d** 320 °C

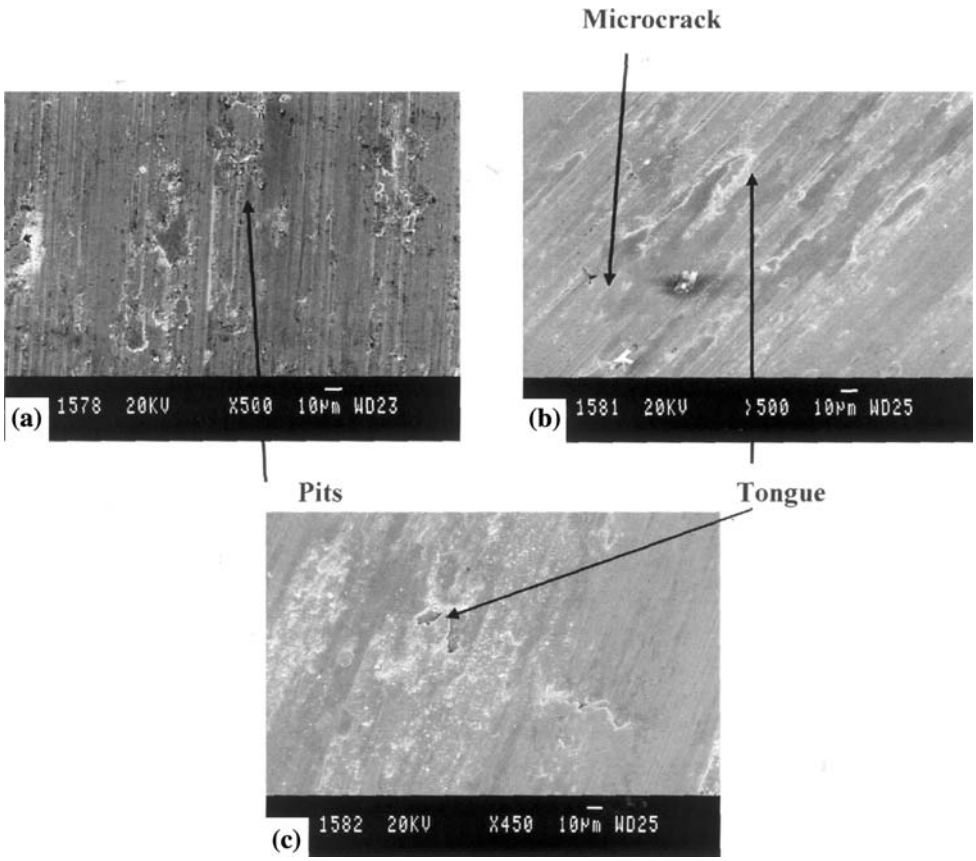

Fig. 12 SEM micrographs of samples subjected to austempering for 2 h at **a** 350 °C, **b** 380 °C and **c** 400 °C

components, due to the asperities, in the direction of rotation. Wear may also occur because of the asperities on the hardened disc, which can gouge out the material from the pin surface. However, the removal of the material by this gouging action would be only a small component of the wear process since the disc is well polished and has a smooth surface.

Under the action of plastic flow and tear, two important properties of the material that will influence its wear behaviour are hardness or strength, and the strain hardening behaviour. Harder the material, greater load will be required for tearing of the material from the surface, or longer run time at a given load. Similarly, higher the strain hardening tendency, more difficult it will be to cause the tear, as the material will tend to flow to a greater extent before it eventually fractures.

As stated earlier, the hardness or strength is the most significant parameter that influences the wear rate. One can assume that wear rate is inversely proportional to the yield strength of the ADI. Another important parameter is the strain hardening ability of the ausferrite. This depends upon the carbon content. It is believed that strain hardening ability of the austenite depends on its carbon content. Greater the carbon content, higher will be strain hardening tendency. It is generally believed that the strain hardening ability of austenite varies as (carbon content)$^{1/2}$.

At low austempering temperatures such as 260–300 °C, fine sheaves of closely spaced ferrite are formed with slivers of austenite in between. Such a microstructure results in high hardness and high strength, which leads to a very good wear resistance. At higher temperatures such as 350–400 °C broad ferrite sheaths with blocky austenite is observed. The coarser microstructure together with the large amount of austenite decreases the strength and hardness. However, such a microstructure can promote the formation of strain induced martensite as explained earlier. It was mentioned while discussing the strain hardening behaviour of the ADIs that the formation of strain induced martensite during tensile deformation leads to enhanced strain hardening. The severe plastic deformation of the wearing surface also leads to the formation of strain induced martensite. Figure 13 shows the microstructure of a region just below the wear surface of a sample subjected to conventional austempering at 400 °C. Martensite can be clearly seen as the dark etching lenticular shaped particles. This strain induced martensite can be expected to improve the wear resistance. As the austempering temperature is increased, the austenite content and its carbon content also increases. Simultaneously, the wear resistance comes down. The wear rate is inversely proportional to the yield strength. Assuming that these three parameters act independently in influencing the wear resistance, one can write

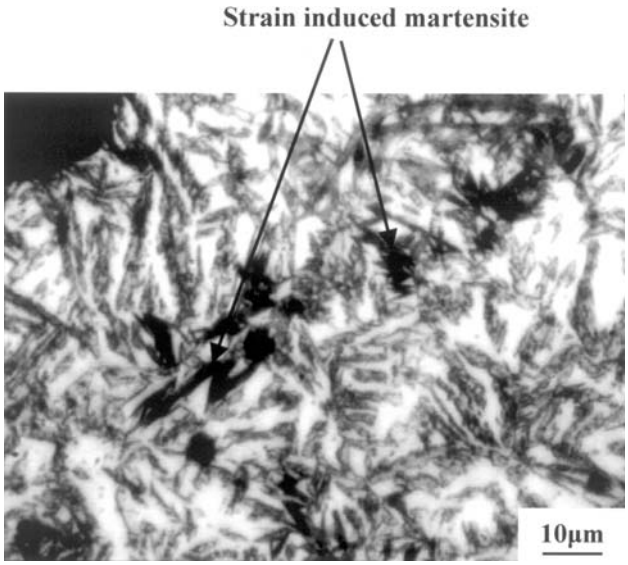

Fig. 13 Microstructure of a region just below the wear surface of ADI austempered at 400 °C, after wear test, showing the presence of martensite

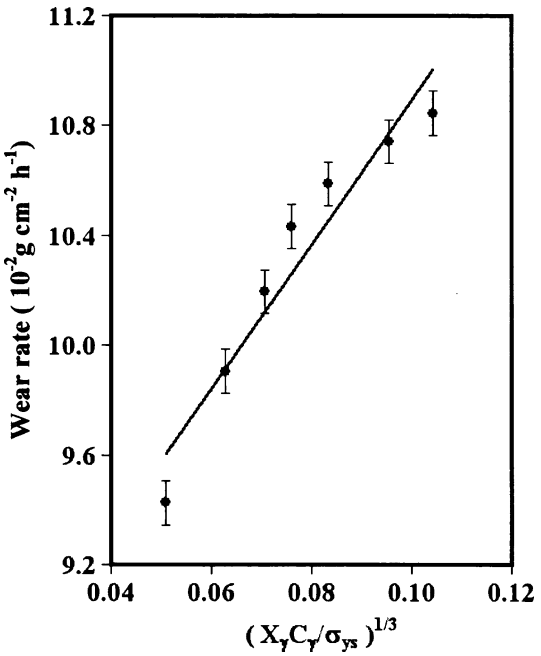

Fig. 14 Variation of wear rate with $(X_\gamma C_\gamma/\sigma_{YS})^{1/3}$

$$W\alpha(X_\gamma C_\gamma/\sigma_{YS})^{1/3} \quad (7)$$

When plotted this gives a good linear relationship between wear rate and $(X_\gamma C_\gamma/\sigma_{YS})^{1/3}$ as shown in Fig. 14 with a correlation coefficient of 0.93.

Conclusions

Following conclusions can be drawn from the present investigation.

1. Strain induced transformation of austenite occurs in samples austempered at higher temperatures. In these samples, the austenite exhibits bulky morphology, large size and relatively low carbon content which are all conducive for transformation to martensite under stress.
2. The tendency to form strain induced martensite increases systematically as austempering temperature is increased.
3. The strain hardening tendency of the ADI increases as austempering temperature is increased. This can be attributed to the increasing propensity to form martensite. Formation of the martensite increases the strength of the matrix, and makes it more difficult to deform.
4. Wear occurred primarily by a process of adhesion and fracture.
5. Wear rate increased with increasing austempering temperature. Formation of strain induced martensite during wear process has a considerable influence on the wear behaviour.
6. Wear rate is dependent on the yield strength, austenite content as well as its carbon content, and obeys the following relationship:

$$W = (X_\gamma C_\gamma/\sigma_{YS})^{1/3}$$

References

1. Dorazil E, Barta B, Munsterova E, Stransky L, Huvar A (1982) AFS Int Cast Metal 7:52
2. Janowak JF, Gundalach RB (1983) AFS Trans 91:377
3. Rouns TN, Rundman KB, Moore DM (1984) AFS Trans 92:815
4. Darwish N, Elliot R (1993) Mater Sci Technol 9:882
5. Moore DJ, Rouns TN, Rundman KB (1985) AFS Trans 93:705
6. Moore DJ, Rouns TN, Rundman KB (1987) AFS Trans 95:765
7. Shea MM, Ryntz EF (1986) AFS Trans 94:683
8. Rundman KB, Moore DJ, Hayrynen KL, Dubensky WJ, Rouns TN (1988) J Heat Treat 5(2):79
9. Bayati H, Elliot R (1995) Mater Sci Technol 11:285
10. Rao PP (1995) J Eng Mater Sci 2:24
11. Bahmani M, Elliot R, Varahram N (1997) J Mater Sci 32:4783. doi:10.1023/A:1018687115732
12. Refaey A, Fatahalla N (2003) J Mater Sci 38:351. doi:10.1023/A:1021177902596
13. Masud L, Martinez R, Simison S, Boeri R (2003) J Mater Sci 38:2971. doi:10.1023/A:1024425727963
14. Lin C, Yang C, Wang J (2003) J Mater Sci 38:1667. doi:10.1023/A:1023211323116
15. Li D, Zhou Z, Sun D (2004) J Mater Sci 39:7119. doi:10.1023/B:JMSC.0000047563.46550.e6
16. Gundalach RB, Janowak JF (1985) Metal Prog 128(2):19
17. Gundalach RB, Janowak JF (1984) Amax Materials Research Center Report No. X G 184-02
18. Harding RA, Gillbert GNJ (1986) British Foundryman, IBF, Conference paper, BFS 79, p 489
19. Schmidt I (1984) Z Metallkd 75:747
20. Shah SM, Verhoeven JD (1986) Wear 113:267

21. Schmidt I, Schuchert A (1987) Z Metallkd 78:871
22. Bartosiewicz L, Krause AR, Alberts FA, Singh I, Putatunda SK (1993) Mater Charact 30:221
23. Shanmugam P, Rao PP, Udupa KR, Venkataraman N (1994) J Mater Sci 29:4933. doi:10.1007/BF00356546
24. Bahmani M, Elliot R, Varahram N (1997) J Mater Sci 32:5383. doi:10.1023/A:1018631314765
25. Lin C, Chang C (2002) J Mater Sci 37:709. doi:10.1023/A:1013827511859
26. Jayamathy M, Vasanth R (2003) SAE Trans 112(3):2066
27. Yasutoune A, Ryohei I, Yoji M, Masahito G (2004) JSME Symposium on Motion and Power Transmissions, p 138
28. Brezina R, Filipek J, Senberger J (2008) Res Agr Eng 50:75
29. Rimmer A (2006) Foundry Trade J 180:58
30. Prado JM, Pujol A, Cullel J, Tartera J (1995) Mater Sci Technol 11:294
31. Owhadi A, Hedjazi J, Davami P (1998) Mater Sci Technol 14:245
32. Ahmadabadi MN, Nategh S, Davami P (1992) J Cast Metals 4:188
33. Shepperson S, Allen C (1988) Wear 121:271
34. Vuorinen J (1986) In: Proceedings of 2nd international conference on austempered ductile iron, Ann Arbor, MI, USA, p 179
35. Gundalach RB, Janowak JF (1986) In: Proceedings of 2nd international conference on austempered ductile iron, Ann Arbor, MI, USA, p 23
36. Gundalach RB, Janowak JF (1987) Wear 11:171
37. Zum-Gahr KH (1979) Metal Prog 116(4):46
38. Velez JM (2001) Wear 251:1315
39. Mohan S, Prakash V, Pathak JP (2002) Wear 252:16
40. Zhou WS, Zhou QD, Meng SK (1993) Wear 162–164:696
41. Daber S, Rao PP (2008) J Mater Sci 43:357. doi:10.1007/s10853-007-2258-6
42. Daber S, Ravishankar KS, Rao PP (2008) J Mater Sci 43:4929. doi:10.1007/s10853-008-2717-8
43. Boutorabi SMA, Young JM, Kondic V (1993) Wear 175:19
44. Ahmadabadi MN, Ghasemi HM, Osia M (1999) Wear 231:293
45. Rundman KB, Klug RC (1982) AFS Trans 90:499
46. Cullity BD (1974) Elements of X-ray diffraction. Addison-Wesley, Reading, MA, p 411
47. Roberts CS (1953) Trans AIME 197:203
48. Rao PP, Putatunda SK (1988) Mater Sci Technol 14:1257
49. Voigt RC, Loper CR (1984) In: Proceedings of Ist international conference on austempered ductile iron, ASM, Metals Park, OH, p 83
50. Rao PP, Putatunda SK (1997) Metal Mater Trans A 28A:1457
51. Rao PP (1995) Indian J Eng Mater Sci 2:24
52. Hayrynen KL, Moore DJ, Rundman KB (1990) AFS Trans 98:471
53. Ali ASH, Uzlov KI, Darwish N, Elliot R (1994) Mater Sci Technol 10:35
54. Hollomon TH (1945) Trans AIME 162:268
55. Tommita Y (1995) J Mater Sci 30:105. doi:10.1007/BF00352138
56. Reisner G, Werner EA, Kerschbaummaur P, Papst I, Fisher FD (1997) J Mater 49(9):62
57. De Meyer M, Vanderschueren D, de Cooman BC (1999) ISIJ Int 39(8):813
58. Bai DQ, Chiro AD, Yue S (1998) Mater Sci Forum 284–286:253
59. Chen HC, Era H, Shimizu M (1989) Metall Trans A 20:437
60. Miihkinen VTT, Edmonds DV (1987) Mater Sci Technol l3:422
61. Brandt ML, Olson GB (1993) Iron Steel Maker 20(5):55
62. Takahashi M, Bhadheshia HKDH (1991) Mater Trans JIM 32:689
63. Wang J, Van der Zwaag S (2001) Metal Mater Trans A 32(6):1527
64. Tsukatani I, Hashimoto S, Inoue T (1991) ISIJ Int 31(9):992